

## High-spin states in $^{92}\text{Nb}^\dagger$

B. A. Brown\* and D. B. Fossan

*Department of Physics, State University of New York, Stony Brook, New York 11794*

(Received 23 February 1977)

High-spin states have been investigated with the  $^{88}\text{Sr}(^7\text{Li}, 3n)^{92}\text{Nb}$  reaction by  $\gamma$ - $\gamma$  coincidence,  $\gamma$ -ray angular distribution, and pulsed beam- $\gamma$  timing measurements with Ge(Li) detectors. Decay schemes, level energies, and spin-parity information were obtained for  $^{92}\text{Nb}$  from the data. The positive-parity yrast level sequence was established up to a  $13^+$  state at 3326 keV. An  $11^-$  isomeric level at 2203 keV was found and observed to have a mean lifetime of  $\tau = 241 \pm 5$  nsec. The  $g$  factor of this isomer was measured to be  $g = 0.88 \pm 0.03$ . The observed properties of levels in  $^{92}\text{Nb}$  are compared with shell-model calculations.

[NUCLEAR REACTIONS  $^{88}\text{Sr}(^7\text{Li}, 3n)$ ,  $E_{\text{Li}} = 34$  MeV; measured  $\gamma$ - $\gamma$  coin,  $\gamma(E, \theta, t)$ ,  
spin rotation in  $B = 11.2$  kG; deduced level scheme in  $^{92}\text{Nb}$ ,  $\gamma$  multipolarities,  
 $T_{1/2}, J^\pi, g$  factor. Natural target, Ge(Li) detectors.]

### I. INTRODUCTION

Reactions with  $^6\text{Li}$  and  $^7\text{Li}$  on the semimagic nucleus  $^{88}\text{Sr}$  ( $Z = 38, N = 50$ ) have been used to investigate high-spin states in the neighboring nuclei, which have simple shell-model configurations. The results and comparisons with theory for  $^{91}\text{Nb}$ ,  $^{91}\text{Zr}$ , and  $^{92}\text{Zr}$  have been presented previously.<sup>1,2</sup> In this paper, the results for  $^{92}\text{Nb}$  ( $Z = 41, N = 51$ ) studied with the  $^{88}\text{Sr}(^7\text{Li}, 3n)$  reaction are presented. High-spin states up to  $\sim 4$  MeV have been found including an isomeric  $J^\pi = 11^-$  level at 2203 keV for which the lifetime and  $g$  factor were measured. A preliminary report on a portion of these results has been made.<sup>3</sup>

The study of odd-odd nuclei is most important for determining the effective proton-neutron residual interaction. In the case of  $^{92}\text{Nb}$ , the six positive parity and two negative parity levels<sup>4</sup> below 500 keV are interpreted in zeroth order as the  $(\pi 1g_{9/2})(\nu 2d_{5/2})$  and  $(\pi 2p_{1/2})(\nu 2d_{5/2})$  multiplets, respectively. These levels should have relatively pure configurations because of the large energy gap above them. The  $^{92}\text{Nb}$  states involving the high-spin three-proton configurations,  $(\pi 1g_{9/2})^3$  and  $(\pi 1g_{9/2})^2(\pi 2p_{1/2})$ , of  $^{91}\text{Nb}$  (Ref. 1) coupled to the odd valence neutron  $(\nu 2d_{5/2})$  have not been previously observed; the maximum  $J^\pi$  values allowed are  $13^+$  and  $11^-$ , respectively.

Much experimental information has been obtained for high-spin states in even-even and even-odd nuclei in this mass region, but very little has been previously reported for the yrast levels of odd-odd nuclei. Odd-odd nuclei, which have large level densities, have been difficult to study with light-ion reactions because of the complex level population. For heavy-ion reactions, which have a selectivity for populating only yrast states, the situation

is different. The number of levels strongly populated in  $^{92}\text{Nb}$  by the  $^{88}\text{Sr}(^7\text{Li}, 3n)$  reaction was approximately the same as the number by similar reactions in the neighboring odd-even nuclei,  $^{91}\text{Nb}$  and  $^{91}\text{Zr}$ .<sup>1</sup>

Previous experiments regarding  $^{92}\text{Nb}$  prior to 1972 are summarized in Nuclear Data Sheets.<sup>5</sup> More recently  $^{92}\text{Nb}$  has been studied with the  $(p, n\gamma)$  and  $(\alpha, n\gamma)$  reactions.<sup>6</sup> In all of these previous studies, no spin assignment higher than that of the ground state spin of  $7^+$  was reported, and hence they have little overlap with the present experiment.

The experimental techniques used in the present measurements are briefly described in Sec. II; they have been discussed in more detail in Ref. 1. The experimental results for the  $^{92}\text{Nb}$  yrast decay are presented in Sec. III, and the comparison with shell-model theory is discussed in Sec. IV.

### II. EXPERIMENTAL TECHNIQUE

Levels in  $^{92}\text{Nb}$  were populated via the fusion-evaporation reaction  $^{88}\text{Sr}(^7\text{Li}, 3n)$ . For most of the measurements, a 34-MeV  $^7\text{Li}(3^+)$  beam, obtained from the Stony Brook FN tandem Van de Graaff accelerator, was incident on a thick natural Sr metal target (82.6%  $^{88}\text{Sr}$ ) which stopped the beam. The beam energy was selected on the basis of  $\gamma$ -ray excitation measurements. Deexcitation  $\gamma$  rays were detected using both large volume Ge(Li) detectors for  $\gamma$  rays with  $100 \text{ keV} < E_\gamma < 3 \text{ MeV}$ , and a small planar intrinsic Ge detector for  $\gamma$  rays with  $20 \text{ keV} < E_\gamma < 200 \text{ keV}$ ; typical energy resolutions were 2.5–3 keV full width at half maximum (FWHM) at 1332 keV, and 0.5 keV at 122 keV, respectively. Three types of experiments were carried out: (1)

$\gamma$ - $\gamma$  coincidence, (2)  $\gamma$ -ray angular distribution, and (3) pulsed-beam- $\gamma$  timing measurements.

Because of the complex nature of the  $\gamma$ -ray spectra from these reactions involving several residual nuclei,  $\gamma$ - $\gamma$  coincidence measurements with a Ge(Li)-Ge(Li) detector combination were required to identify the  $\gamma$ -ray cascades. To obtain information on the spins of the levels and the  $\gamma$ -ray multiplicities as well as the  $\gamma$ -ray intensities  $I_\gamma$ ,  $\gamma$ -ray angular distributions were measured in singles at seven angles between  $0^\circ$  and  $90^\circ$ . The photopeak areas were extracted and fitted to  $W(\theta) = I_\gamma(1 + A_2 P_2 + A_4 P_4)$ , where the  $P_k$  are the Legendre polynomials. Spin assignments were obtained from  $W(\theta)$ , lifetime, and  $I_\gamma$  results. Finally, the observation of delayed  $\gamma$  rays with pulsed-beam timing allows the location of isomeric states and the study of their decay modes. Pulsed-beam measurements using the Ge(Li) and planar Ge detectors with overall time resolutions of  $\sim 8$  nsec FWHM were made with pulse repetition periods of 500 nsec and 1  $\mu\text{sec}$ .

### III. RESULTS

The singles  $\gamma$ -ray spectrum from the reactions induced by a 34-MeV  $^7\text{Li}$  beam and thick natural Sr metal target is shown in Fig. 2 of Ref. 2. The  $\gamma$  rays belonging to  $^{92}\text{Nb}$  were identified by their excitation function as well as a comparison of the in-

TABLE I. Results of  $\gamma$ - $\gamma$  coincidence measurements for  $^{92}\text{Nb}$   $\gamma$  rays.

$\gamma$ ray in gate (keV)	Coincident $\gamma$ rays <sup>a,b</sup> (keV)
116	(598), (1066), 2087
123	357
142	328, 501, (511), 763, 1129( $^{90}\text{Zr}$ ), (2087)
148	194, 328, 471, (511), 763, (1066), (1553), 2087
150	
163	919, ( $\sim 1030$ ), $\sim 1082$
194	$\sim 603$ , 1791( $^{91}\text{Nb}$ )
328	148, (471), 501, (511), 711, 763, 2087, 2287
471	148, 317, <sup>c</sup> 328, 344, <sup>c</sup> 711, 763, 777, <sup>c</sup> 934, <sup>c</sup> 1239, <sup>c</sup> 1658, <sup>c</sup> 2087
501	116, 142, 148, (511), 1444, (1586)
711	328, 471, 2287
763	(142), 148, 328, 471, 501, 2087
1444	(96), (202), 501
2087	116, 148, 328, 471, 763
2287	328, 356( $^{91}\text{Nb}$ ), 711, 819( $^{91}\text{Nb}$ )

<sup>a</sup>The present experiment was not sensitive to coincident  $\gamma$  rays below about 200 keV for the gated  $\gamma$  rays with  $E_\gamma \leq 194$  keV.

<sup>b</sup>Coincident  $\gamma$  rays which are uncertain are put in parentheses.

<sup>c</sup>These  $\gamma$  rays are probably not from  $^{92}\text{Nb}$ .

tensities of  $\gamma$  rays from the  $^7\text{Li}$  and  $^6\text{Li}$  reactions on  $^{88}\text{Sr}$  at 34 MeV. In the  $^6\text{Li} + ^{88}\text{Sr}$  reaction<sup>1</sup> at 34 MeV, it was observed that the cross section was peaked for the evaporation of three neutrons ( $3n$ ) leading to  $^{91}\text{Nb}$ , as expected from theoretical estimates,<sup>7</sup> and that the ratio of the  $3n$  to the  $p2n$  cross sections was about 3 to 1. It is then estimated that, in the  $^7\text{Li} + ^{88}\text{Sr}$  reaction at 34 MeV, the  $3n$  evaporation leading to  $^{92}\text{Nb}$  and the  $3n$  to  $p2n$  cross-section ratio should have similar characteristics. From these considerations, a coincident set of  $\gamma$  rays which are the strongest  $\gamma$  rays appearing in the  $^7\text{Li} + ^{88}\text{Sr}$  reaction are assigned to  $^{92}\text{Nb}$ . Two new  $\gamma$  rays, as well as the previously known 501-

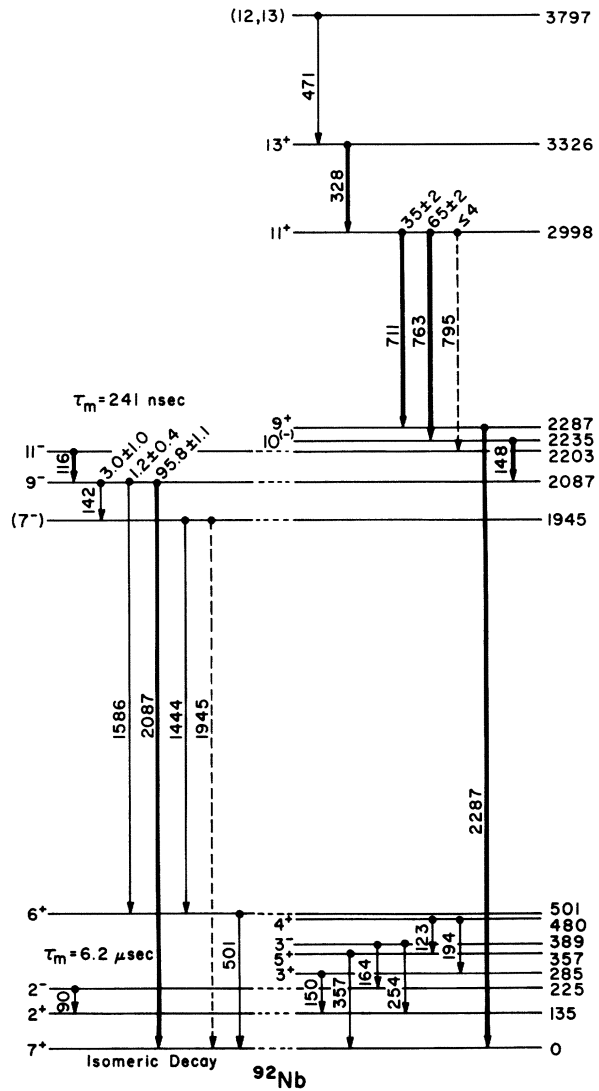


FIG. 1. The decay scheme for  $^{92}\text{Nb}$  high-spin levels from the present work. The tentative levels from the present work at 1309, 1420, and 1472 keV are not included. The non-yrast levels below 501 keV are from Refs. 4-6.

TABLE II. Properties of  $\gamma$  rays assigned to transitions in  $^{92}\text{Nb}$  from the  $^{88}\text{Sr}(^7\text{Li}, 3n)$  reaction.

$E_\gamma$ (keV)	Intensity (%) (relative to 2087 keV)	Transition assignment			
		$A_2$	$A_4$	$E_i$ (keV) $\rightarrow$ $E_f$ (keV)	$J_i \rightarrow J_f$
90.2 $\pm$ 0.2	Doublet			226 $\rightarrow$ 135	2 <sup>-</sup> $\rightarrow$ 2 <sup>+</sup>
115.8 $\pm$ 0.2	18	0.28 $\pm$ 0.02	-0.04 $\pm$ 0.03	2203 $\rightarrow$ 2087	11 <sup>-</sup> $\rightarrow$ 9 <sup>-</sup>
122.5 $\pm$ 0.2	Doublet			481 $\rightarrow$ 358	4 <sup>+</sup> $\rightarrow$ 5 <sup>+</sup>
142.2 $\pm$ 0.2	3 <sup>a, b</sup>			2087 $\rightarrow$ 1946	9 <sup>-</sup> $\rightarrow$ 7 <sup>-</sup>
148.2 $\pm$ 0.2	44 <sup>a</sup> }	-0.21 $\pm$ 0.02	0.02 $\pm$ 0.02	2235 $\rightarrow$ 2087	10 <sup>(-)</sup> $\rightarrow$ 9 <sup>-</sup>
149.9 $\pm$ 0.2	22 <sup>a</sup> }			286 $\rightarrow$ 135	3 <sup>+</sup> $\rightarrow$ 2 <sup>+</sup>
163.8 $\pm$ 0.2	20	-0.17 $\pm$ 0.03	0.04 $\pm$ 0.03	390 $\rightarrow$ 226	3 <sup>-</sup> $\rightarrow$ 2 <sup>-</sup>
194.4 $\pm$ 0.2	Doublet			481 $\rightarrow$ 286	4 <sup>+</sup> $\rightarrow$ 3 <sup>+</sup>
254 $\pm$ 1	Weak			390 $\rightarrow$ 135	3 <sup>-</sup> $\rightarrow$ 2 <sup>+</sup>
327.7 $\pm$ 0.2	43	0.35 $\pm$ 0.01	-0.10 $\pm$ 0.01	3326 $\rightarrow$ 2998	13 <sup>+</sup> $\rightarrow$ 11 <sup>+</sup>
357 $\pm$ 1	Doublet	(0.21 $\pm$ 0.03)	-0.04 $\pm$ 0.04)	358 $\rightarrow$ 0	5 <sup>+</sup> $\rightarrow$ 7 <sup>+</sup>
471 $\pm$ 1	Doublet			3797 $\rightarrow$ 3326	(12, 13) $\rightarrow$ 13 <sup>+</sup>
501.0 $\pm$ 0.3	41	-0.02 $\pm$ 0.03	-0.04 $\pm$ 0.03	501 $\rightarrow$ 0	6 <sup>+</sup> $\rightarrow$ 7 <sup>+</sup>
711.1 $\pm$ 0.2	20	0.33 $\pm$ 0.04	-0.11 $\pm$ 0.05	2998 $\rightarrow$ 2287	11 <sup>+</sup> $\rightarrow$ 9 <sup>+</sup>
762.5 $\pm$ 0.2	36	-0.20 $\pm$ 0.01	-0.00 $\pm$ 0.02	2998 $\rightarrow$ 2235	11 <sup>+</sup> $\rightarrow$ 10 <sup>(-)</sup>
1444.5 $\pm$ 1.0	5 <sup>b</sup>			1946 $\rightarrow$ 501	7 <sup>-</sup> $\rightarrow$ 6 <sup>+</sup>
1586.4 $\pm$ 1.0	Weak <sup>b</sup>			2087 $\rightarrow$ 501	9 <sup>-</sup> $\rightarrow$ 6 <sup>+</sup>
1945 $\pm$ 1	$\leq$ 10 (doublet)			(1946 $\rightarrow$ 0)	7 <sup>-</sup> $\rightarrow$ 7 <sup>+</sup> )
2087.4 $\pm$ 0.4	100	0.083 $\pm$ 0.015	-0.128 $\pm$ 0.016 <sup>c</sup>	2087 $\rightarrow$ 0	9 <sup>-</sup> $\rightarrow$ 7 <sup>+</sup>
2287.2 $\pm$ 1.0	$\sim$ 40 (doublet)	(0.30 $\pm$ 0.02)	-0.06 $\pm$ 0.02) <sup>d</sup>	2287 $\rightarrow$ 0	9 <sup>+</sup> $\rightarrow$ 7 <sup>+</sup>

<sup>a</sup> Intensities at 90° observed with the intrinsic Ge detector (Fig. 3) relative to the integrated intensity of the 148.2 + 149.9-keV  $\gamma$  rays observed with the Ge(Li) detector.

<sup>b</sup> The branching ratios shown in Fig. 1 involving these transitions were obtained from the delayed intensities at 90° of the 1444-, 1586-, and 2087-keV transitions corrected for the expected angular distributions.

<sup>c</sup>  $A_6 = 0.111 \pm 0.019$ .

<sup>d</sup> The angular distribution coefficients here are for the sum of the 2287-keV  $^{92}\text{Nb}$  and 2291-keV  $^{91}\text{Nb}$   $\gamma$  rays. However, the fact that the line shape for these two  $\gamma$  rays remains the same at all angles indicates that these coefficients are valid for both  $\gamma$  rays.

keV  $\gamma$  ray, represent transitions to the  $^{92}\text{Nb}$  ground state. With these assignments together with previously established  $\gamma$ -ray transitions to the ground states of other nuclei in this region, the relative population yields determined from ground-state transitions were  $^{92}\text{Nb}(11)$ ,  $^{89}\text{Y}(7)$ ,  $^{91}\text{Nb}(6)$ ,  $^{92}\text{Zr}(3)$ ,  $^{90}\text{Zr}(2)$ ,  $^{90}\text{Y}(2)$ ,  $^{91}\text{Zr}(1)$ , and  $^{88}\text{Y}(1)$ . Our results for  $^{92}\text{Zr}$  have been previously reported.<sup>2</sup>

A summary of the properties of  $\gamma$ -ray transitions assigned to  $^{92}\text{Nb}$  is given in Table I and the deduced  $^{92}\text{Nb}$  level scheme is shown in Fig. 1. A list of the  $\gamma$ - $\gamma$  coincidence results is given in Table II; the coincidence spectra for the principle  $^{92}\text{Nb}$   $\gamma$  rays are shown in Fig. 2. The prompt decay scheme based on the angular distribution and coincidence measurements is discussed in Sec. III A.

The delayed  $\gamma$ -ray measurements established an isomeric 11<sup>-</sup> level at 2203 keV ( $\tau = 241 \pm 5$  nsec) which decays via an 11<sup>-</sup>  $\rightarrow$  9<sup>-</sup>  $\rightarrow$  7<sup>+</sup> ground state (g.s.) cascade. The delayed  $\gamma$  spectra for low energy  $\gamma$  rays observed with a planar intrinsic Ge detector are shown in Fig. 3. The isomeric decay, including the  $g$ -factor measurement for the 11<sup>-</sup> level, is discussed in Sec. III B.

#### A. Prompt decay

The dominant decay pattern obtained from the  $\gamma$ - $\gamma$  coincidence measurements and singles intensities consists of two  $\gamma$ -ray cascades to the 7<sup>+</sup> ground state both originating with a 328-keV  $\gamma$  ray (see Fig. 1). The angular distribution coefficients for the  $\gamma$  rays in the 328-711-2287 cascade are all very similar with  $A_2 \approx 0.3$  and  $A_4 \approx -0.1$ , which is the signature of a stretched  $L = 2$  cascade. This information together with the prompt lifetimes and regularly decreasing intensities of the cascade  $\gamma$  rays strongly suggest spin assignments of 9<sup>+</sup>, 11<sup>+</sup>, and 13<sup>+</sup> for the 2287-, 2998-, and 3326-keV levels, respectively.

The second cascade to the ground state involves the 328, 763, 148, and 2087 keV  $\gamma$  rays. In order to fit the angular distribution of the 2087 keV  $\gamma$  ray a  $P_6(\cos\theta)$  term was needed ( $\chi^2 = 9.2$  without and  $\chi^2 = 1.3$  with this term) which indicates a strong  $L = 3$  component in this transition. The only likely possibilities for this prompt ( $\tau \leq 10$  nsec) transition are 10<sup>-</sup>  $\rightarrow$  7<sup>+</sup> or 9<sup>-</sup>  $\rightarrow$  7<sup>+</sup>. The angular distribution can be fitted only with a 9<sup>-</sup>  $\rightarrow$  7<sup>+</sup> assignment for a mixing ratio  $\delta(E3/M2) = 11 \pm 2$  and a Gaussian width

for the population parameters of the initial state<sup>1</sup>  $\sigma = 2.35 \pm 0.20$ . This value of  $\sigma$  is consistent with the value  $\sigma \approx 2.8$  needed for the angular distributions of the pure  $E1$  and  $E2$  transitions.

The 763- and 148-keV  $\gamma$  rays, which form a cascade between the 2998-keV  $11^+$  and 2087-keV  $9^-$  levels via an intermediate level at 2235 keV, have stretched dipole angular distributions,  $A_4 \approx -0.2$  and  $A_4 \approx 0$ . This leads to a spin assignment of  $J = 10$  for the 2235-keV level. A negative parity for this level is suggested by the fact that the competition between the  $11^+ \rightarrow 9^+$  and  $11^+ \rightarrow 10^-$  branches is consistent with typical  $E2$  enhancements compared to  $E1$  hindrances in the mass-90 region;  $\Gamma(E2)/\Gamma(E1) = CE_{\gamma^5}(E2)/E_{\gamma^3}(E1)$  has empirical values of

$C = 1-100 \text{ MeV}^{-2}$  compared with the Weisskopf estimate of  $C = 1.4 \times 10^{-5} \text{ MeV}^{-2}$ . A  $10^+$  assignment would require that both the  $M1$  and  $E2$  components of a  $11^+ \rightarrow 10^+$  transition be hindered, however, the positive parity assignment cannot be ruled out on this basis.

A weak 471-keV  $\gamma$  ray is in coincidence with the  $\gamma$  rays in the strong cascades discussed above and hence most probably represents feeding of the 3362-keV level by a non-yrast level at 3797 keV. The 471-keV  $\gamma$ -ray peak must be a doublet since it is in coincidence with other  $\gamma$  rays which cannot be in  $^{92}\text{Nb}$  as they also appear in the  $^{88}\text{Sr} + ^6\text{Li}$  data (the dominant  $^{92}\text{Nb}$   $\gamma$  rays do not appear with any significant intensity in the  $^{88}\text{Sr} + ^6\text{Li}$  reaction).

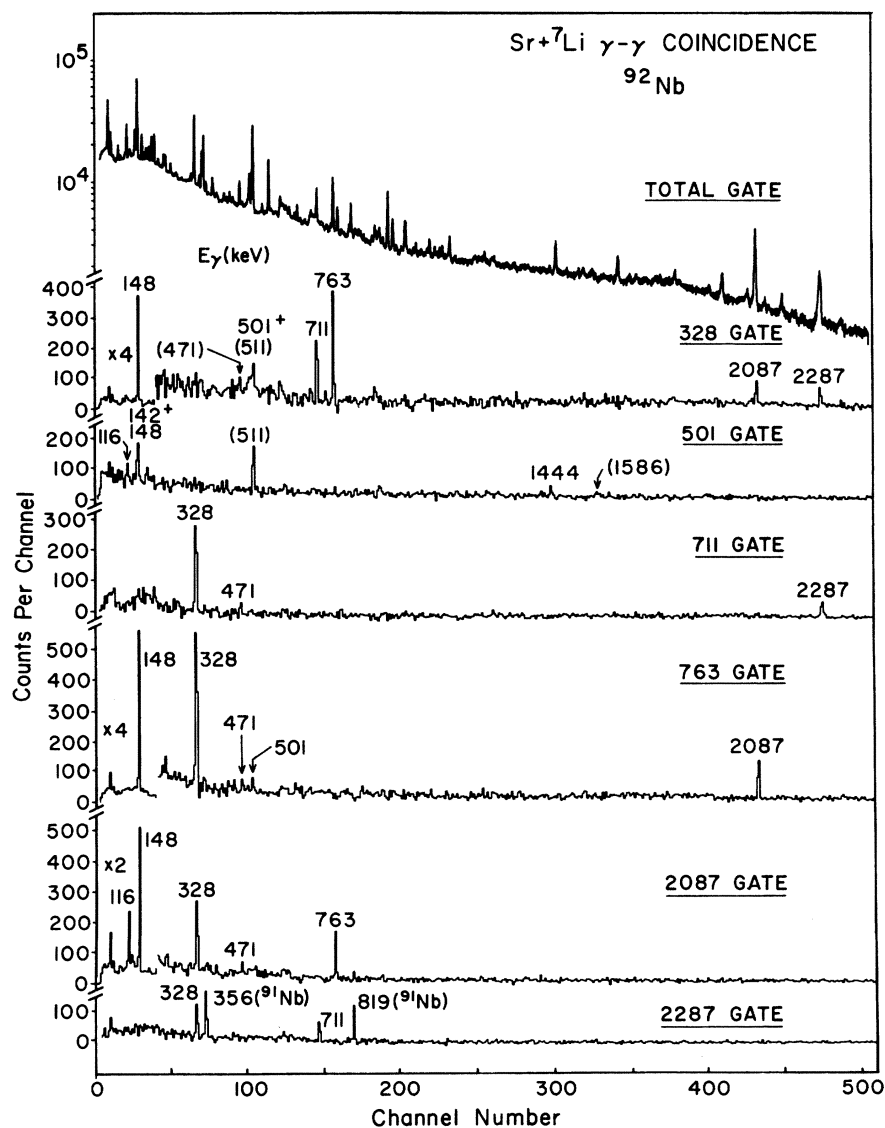


FIG. 2.  $\gamma$ - $\gamma$  coincidence spectra for selected  $^{92}\text{Nb}$   $\gamma$  rays. See Table I for a complete listing of the coincidence results.

Since angular distribution information for the 471-keV  $\gamma$  ray cannot be attributed entirely to  $^{92}\text{Nb}$ , a tentative spin assignment of  $J=(12, 13)$  is made on the basis of its weak non-yrast character.

All of the  $\gamma$  rays which have been previously reported for the low lying multiplets with  $J^\pi=2^+-7^+$  and  $2^--3^-$  were observed in the  $\gamma$  ray singles spectrum. Most of these are observed in the planar Ge spectrum shown in Fig. 3. Some of these  $\gamma$  rays appear as doublets with known transitions in other residual nuclei of the  $\text{Sr}+^7\text{Li}$  reaction: 90 keV ( $^{91}\text{Zr}$ ), 122 keV ( $^{90}\text{Nb}$ ), 194 keV ( $^{91}\text{Nb}$ ), and 357 keV ( $^{91}\text{Nb}$ ). None of the  $^{92}\text{Nb}$   $\gamma$  rays which originate

from non-yrast levels are in strong coincidence with the high-spin cascades discussed above. The  $\gamma$  rays with energies of 919, 1030, and 1082 keV in coincidence with the 163-keV  $3^--2^-$  transition suggest levels in  $^{92}\text{Nb}$  at about 1309, 1420, and 1472 keV with spins of  $3^-$ ,  $4^-$ , or  $5^-$ . However, due to the complexity of the  $\gamma$  spectra these levels cannot be entirely justified unless additional information from their  $\gamma$  decay or observation in particle reactions can be obtained. The transitions from the 1309- and 1420-keV levels to the 389-keV level were also recently observed in  $(p, n\gamma)$  and  $(\alpha, n\gamma)$ .<sup>6</sup>

Several weak  $\gamma$  rays are in coincidence with the

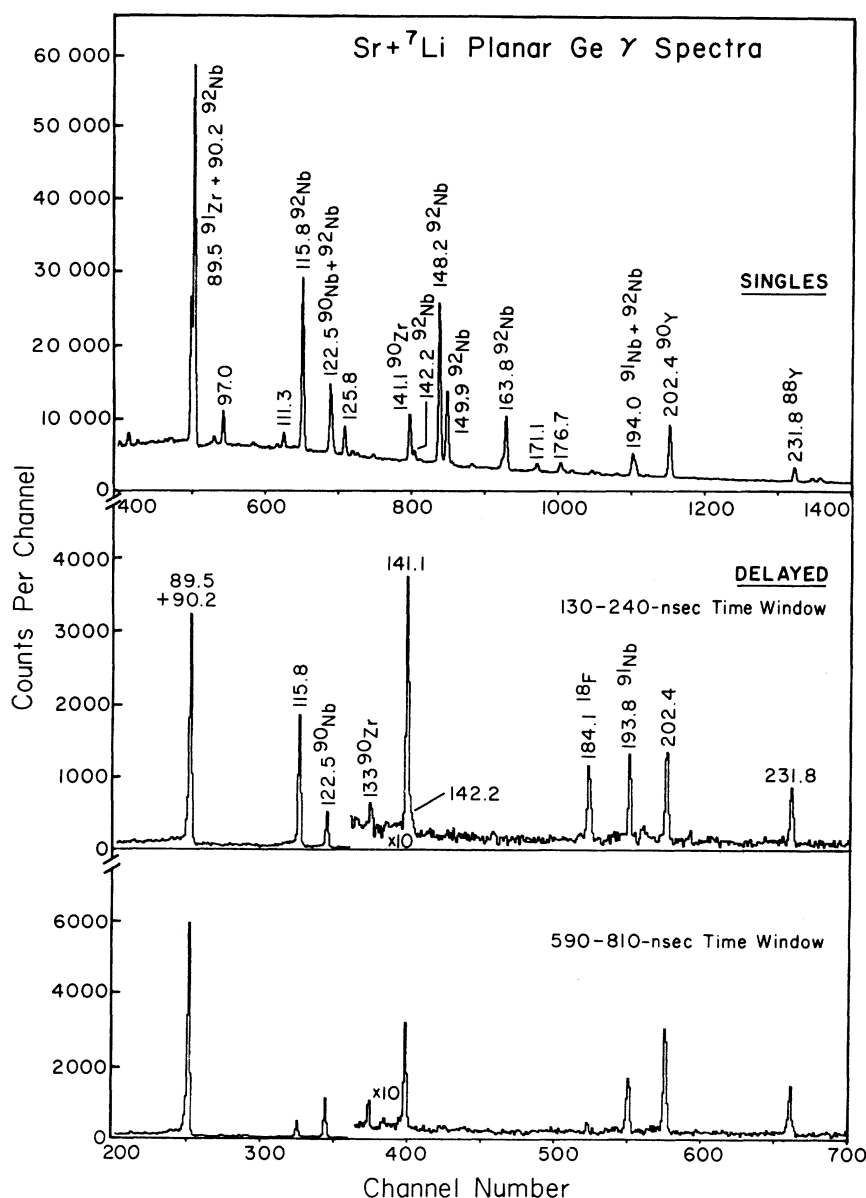


FIG. 3. Prompt and delayed planar Ge spectra from the  $\text{Sr}+^7\text{Li}$  reactions.

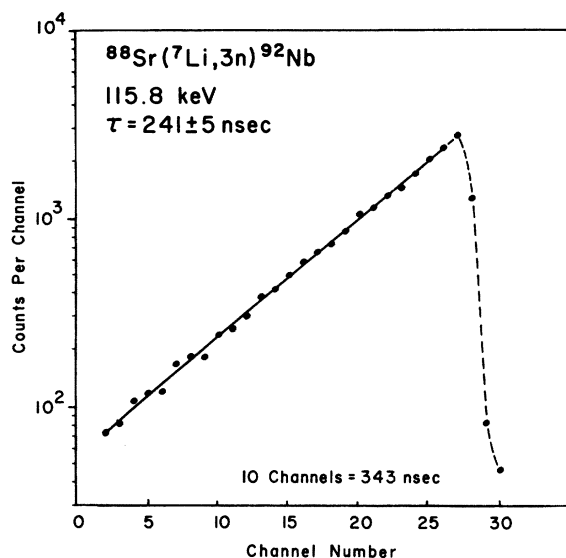


FIG. 4. Time spectrum for the  $^{92}\text{Nb}$  115.8-keV  $\gamma$  ray observed with the planar Ge detector. The delayed spectrum of the Compton background for a region near the photopeak has been subtracted. The solid line is the fitted exponential decay.

501-keV  $6^+ \rightarrow$  g.s.  $7^+$  transition. The 1586-keV  $\gamma$  ray represents the 2087-keV  $9^- \rightarrow$  501-keV  $6^+$  transition. The 142- and 1444-keV  $\gamma$  rays represent another weak cascade of the  $9^-$  level to the  $6^+$  level via an intermediate level at 1945 keV. The tentative spin and parity assignment for this state is  $7^-$ . The branching ratios for the 2087-keV  $9^-$  level shown in Fig. 1 were obtained from the relative intensities of the delayed components of the 1444-, 1586-, and 2087-keV  $\gamma$  rays. The delayed components originate from the feeding of the  $9^-$  level by the  $11^-$  iso-

meric level which will be discussed in the next section.

#### B. 11 isomeric level

The 116- and 2087-keV  $\gamma$  rays appear strongly in the pulsed-beam- $\gamma$  delayed spectra with the same lifetime slope; the averaged mean lifetime extracted is  $\tau = 241 \pm 5$  nsec. The decay curve for the 116-keV  $\gamma$  ray obtained with the planar Ge detector is shown in Fig. 4. The 2087-keV  $\gamma$  ray had an additional prompt component whereas the 116-keV  $\gamma$  ray did not have a prompt component, which establishes the isomeric level at 2203 keV. The angular distribution of the 116-keV  $\gamma$  ray determines this as a stretched  $E2$  transition which gives an assignment of  $J^\pi = 11^-$  for the 2203-keV level. Using the theoretical value of  $\alpha = 0.690$  for the internal conversion coefficient,<sup>8</sup> a  $B(E2) = 98 \pm 3 e^2 \text{fm}^4$  is obtained for the  $11^- \rightarrow 9^-$  transition.

The  $g$  factor of the  $11^-$  level was measured with the time-differential perturbed-angular distribution technique. The planar Ge detector was placed at  $45^\circ$  relative to the beam and an external field of 11.20 kG was applied. The perturbed decay curve was fitted to the functional form

$$N(t) = Ne^{-t/\tau} [1 + b e^{-t/\tau_R} \cos(2\omega_L t)],$$

where  $\tau = 241 \pm 5$  nsec is the lifetime of the isomeric level,  $\tau_R$  is the relaxation time due to fluctuating hyperfine fields, and  $\omega_L$  is the Larmor precession frequency. The data together with the fit are shown after dividing by the factor  $Ne^{-t/\tau}$  in Fig. 5. The results of the fit were  $\omega_L = 0.0472 \pm 0.0014 \text{ nsec}^{-1}$  and  $\tau_R = 360 \pm 100$  nsec. The resulting uncorrected  $g$  factor for the 2203-keV level is  $0.88 \pm 0.03$ . The combined diamagnetic and Knight-shift correction is estimated to be negligible [ $\sim (0 \pm 1)\%$ ].

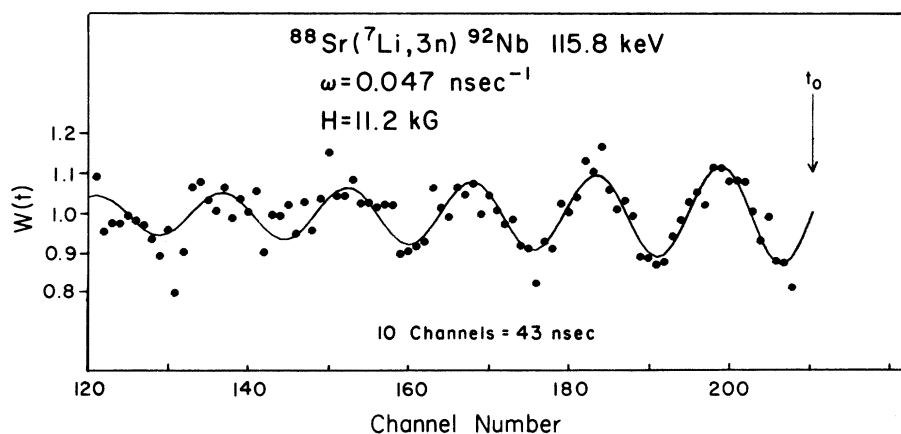


FIG. 5. Perturbed time spectra for the  $^{92}\text{Nb}$  115.8-keV  $\gamma$  ray with the target in an external magnetic field, after dividing by the exponential decay  $Ne^{-t/\tau}$ , where  $\tau = 241$  nsec. The solid line is the fit to the function  $[1 + b e^{-t/\tau_R} \cos(2\omega_L t)]$ , where  $\tau_R$  is the relaxation time and  $\omega_L$  is the Larmor precession frequency.

## IV. DISCUSSION

Most of the levels in  $^{92}\text{Nb}$  below about 4 MeV should be accounted for by three protons distributed in the  $1g_{9/2}$  and  $2p_{1/2}$  orbitals and one neutron in the  $2d_{5/2}$ ,  $3s_{1/2}$ ,  $2d_{3/2}$ ,  $1h_{11/2}$ , or  $1g_{7/2}$  orbit outside a  $^{88}\text{Sr}$  closed core. In particular, the high-spin states arise from the multiplets found from coupling the three-proton yrast levels in  $^{91}\text{Nb}$  (Ref. 1) to the neutron in the  $2d_{5/2}$  or  $1h_{11/2}$  orbital. The stretched configurations for  $^{91}\text{Nb} \times 2d_{5/2}$  give rise to level spacings in  $^{92}\text{Nb}$  which are remarkably similar to the spacings in  $^{91}\text{Nb}$ . The following levels from the nuclear pair [ $^{91}\text{Nb}$ - $^{92}\text{Nb}$ ] can thus be associated: [0 keV  $\frac{9}{2}^+$ -0 keV  $7^+$ ], [1791 keV  $\frac{9}{2}^-$ -1945 keV ( $7^-$ )], [1985 keV  $\frac{13}{2}^-$ -2087 keV  $9^-$ ], [2035 keV  $\frac{11}{2}^-$ -2203 keV  $11^-$ ], [2291 keV  $\frac{13}{2}^-$ -2287 keV  $9^+$ ], [3310 keV  $\frac{11}{2}^+$ -2998 keV  $11^+$ ], and [3467 keV  $\frac{13}{2}^+$ -3326 keV  $13^+$ ]. This weak coupling appearance was also found in the comparison of even-even  $N=50$  nuclei to even-odd  $N=51$  nuclei (see Fig. 10 in Ref. 1). Finally, the 2235-keV  $10^{(-)}$  level can be associated with the stretched [ $^{91}\text{Nb}(\text{g.s.}) \times 1h_{11/2}$ ]  $J=J_{\text{max}}$  configuration or the [ $^{91}\text{Nb}(\frac{17}{2}^-) \times 2d_{5/2}$ ]  $J=J_{\text{max}}-1$  configuration which have unperturbed energies of 2170 and 2035 keV, respectively.

Recent shell-model calculations for  $^{92}\text{Nb}$  have been carried out by Gloeckner.<sup>9,10</sup> For this calculation, the proton-proton interaction matrix elements within the  $g_{9/2}$ - $p_{1/2}$  model space were taken from the seniority conserving interaction needed to fit the energy levels of  $N=50$  nuclei.<sup>11</sup> The proton-neutron matrix elements involving neutrons in the  $d_{5/2}$ - $s_{1/2}$  model space were determined by a fit to levels of  $N=51$  nuclei (see column 3 of Table 2 in Ref. 9). The resulting theoretical  $^{92}\text{Nb}$  energy levels<sup>10</sup> are compared with experiment in Fig. 6. The weak coupling appearance discussed above is also seen in the theoretical energy levels; despite this, the wave functions have large amplitudes of other components representing nonstretched configurations, which have a large effect on some of the electromagnetic properties as will be discussed below. The calculated energies of the  $9^-$ ,  $10^-$ , and  $11^-$  levels are not in very good agreement with experiment which may be due to the fact that the  $1h_{11/2}$  neutron orbital was not included in the calculation.

The electromagnetic properties give a further test of the nuclear wave functions. The measured  $g$  factor of the 2203-keV  $11^-$  level can be compared with that expected for the stretched  $^{91}\text{Nb}(\frac{17}{2}^-) \times 2d_{5/2}$  configuration which is the only configuration possible within Gloeckner's model space. The additivity property for the effective magnetic moment operator implies that,

$$\mu[^{92}\text{Nb}(11^-)] = \mu[^{91}\text{Nb}(\frac{17}{2}^-)] + \mu[2d_{5/2}].$$

Using the  $^{91}\text{Zr}$  ground state moment for the  $2d_{5/2}$  neutron orbital,<sup>12</sup>  $\mu[^{91}\text{Zr}(\frac{9}{2}^+)] = -1.303\mu_N$ , and a recently measured value for the  $^{91}\text{Nb}$  moment,<sup>13</sup>  $\mu[^{91}\text{Nb}(\frac{17}{2}^-)] = (10.84 \pm 0.14)\mu_N$ , the additivity relation gives  $\mu[^{92}\text{Nb}(11^-)] = (9.54 \pm 0.14)\mu_N$  or  $g = 0.867 \pm 0.013$  in agreement with the  $^{92}\text{Nb}$  experimental

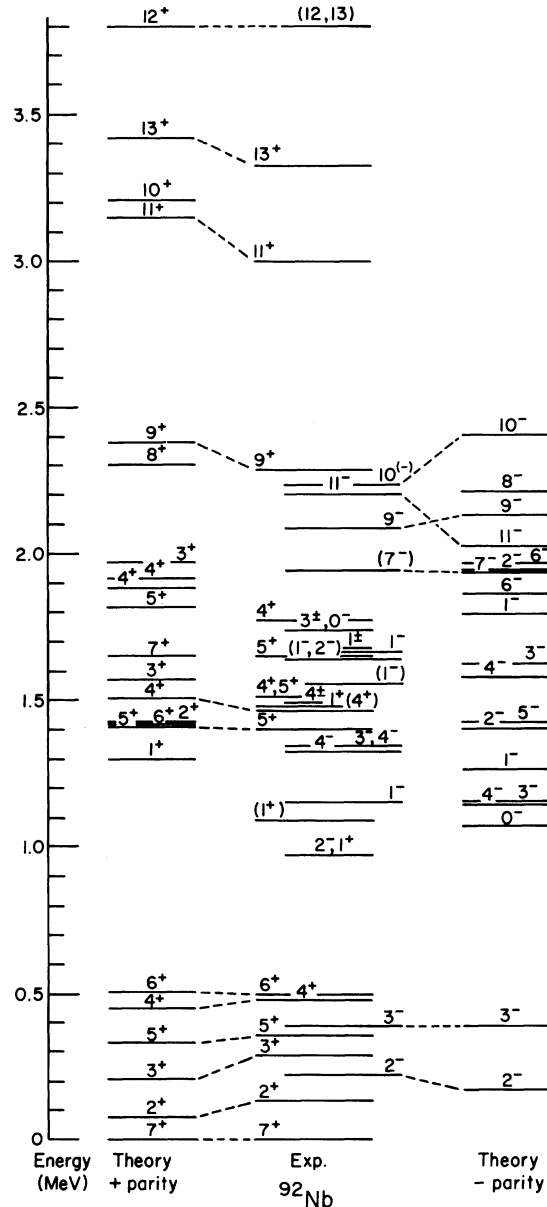


FIG. 6. Comparison of the experimental and theoretical energy levels for  $^{92}\text{Nb}$ . The experimental information is from the present work and other  $\gamma$ -ray studies in Refs. 4-6. [The tentative levels from the present work at 1309, 1420, and 1472 keV and information from the very recent work of Davidson *et al.*, Ref. 6 are not included.] The theoretical energy levels were calculated by Gloeckner (Refs. 9 and 10) and are discussed in Sec. IV of the text.

value  $g_{\text{exp}} = 0.88 \pm 0.03$ . This comparison supports the  $^{91}\text{Nb}(\frac{11}{2}^-) \times d_{5/2}$  configuration for the  $11^-$  isomeric state.

The  $B(E2)$  value for the  $^{92}\text{Nb } 11^- \rightarrow 9^-$  transition and its comparison with  $B(E2)$  values for other  $N = 51$  nuclei have been discussed in Ref. 1. Here we remark on the weak coupling nature of the  $E2$  matrix element. Assuming that the  $11^-$  and  $9^-$  states have the pure configurations  $^{91}\text{Nb}(\frac{11}{2}^-) \times d_{5/2}$  and  $^{91}\text{Nb}(\frac{13}{2}^-) \times d_{5/2}$ , respectively, the  $B(E2)$  values for the  $^{92}\text{Nb } 11^- \rightarrow 9^-$  and  $^{91}\text{Nb } \frac{11}{2}^- \rightarrow \frac{13}{2}^-$  transitions should be equal. However, experimentally the  $B(E2)[^{92}\text{Nb } 11^- \rightarrow 9^-] = 98 \pm 3 \text{ e}^2 \text{ fm}^4$  and the  $B(E2)[^{91}\text{Nb } \frac{11}{2}^- \rightarrow \frac{13}{2}^-] = 32.0 \pm 1.9 \text{ e}^2 \text{ fm}^4$ .<sup>1</sup> This dif-

ference can be partly accounted for by the fact that the shell-model wave function for the  $^{92}\text{Nb } 9^-$  state has a large  $[^{91}\text{Nb}(\frac{11}{2}^-) \times d_{5/2}]J = J_{\text{max}} - 2$  component which contributes coherently to the  $E2$  matrix elements; Gloeckner obtains  $(B(E2)_{\text{th}})^{1/2} = 3.61e_p + 3.03e_n$  compared with the pure configuration value of  $(B(E2)_{\text{th}})^{1/2} = 4.06e_p$ . Using Gloeckner's matrix element and an experimental proton effective charge of  $e_p = 1.39$  from the  $^{91}\text{Nb } \frac{11}{2}^- \rightarrow \frac{13}{2}^-$  transition, the  $^{92}\text{Nb } 11^- \rightarrow 9^- B(E2)$  value requires a neutron effective charge of  $e_n = 1.61 \pm 0.06$  which is still large compared with the average for other  $N = 51$  nuclei<sup>1</sup> of  $e_n \approx 1.0$ . This difference is not understood at present.

†Work supported in part by the National Science Foundation.

\*Present address: Cyclotron Laboratory, Michigan State University, East Lansing, Michigan 48824.

<sup>1</sup>B. A. Brown, P. M. S. Lesser, and D. B. Fossan, Phys. Rev. C **13**, 1900 (1976).

<sup>2</sup>B. A. Brown, D. B. Fossan, P. M. S. Lesser, and A. R. Poletti, Phys. Rev. C **14**, 602 (1976).

<sup>3</sup>B. A. Brown, P. M. S. Lesser, and D. B. Fossan, Bull. Am. Phys. Soc. **19**, 1003 (1974).

<sup>4</sup>S. Cochavi and D. B. Fossan, Phys. Rev. C **3**, 275 (1971).

<sup>5</sup>D. C. Kocher and D. J. Horen, Nucl. Data Sheets **B7**, 229 (1972).

<sup>6</sup>I. Kumabe, S. Matsuki, S. Nakamura, M. Hyakutake, M. Matoba, and T. Sato, Nucl. Phys. **A218**, 201 (1974); J. J. Kent and S. L. Blatt, *ibid.* **A255**, 296 (1975); J. M. Davidson, D. M. Sheppard, P. W. Green, and

J. A. Kuehner, Phys. Rev. C **15**, 104 (1977).

<sup>7</sup>J. O. Newton, in *Nuclear Spectroscopy and Reactions, Part C*, edited by J. Cerny (Academic, New York, 1974), pp. 185-227; J. R. Grover, Phys. Rev. **157**, 832 (1967).

<sup>8</sup>R. S. Hager and E. C. Seltzer, Nucl. Data **A4**, 1 (1968).

<sup>9</sup>D. H. Gloeckner, Nucl. Phys. **A253**, 301 (1975).

<sup>10</sup>D. H. Gloeckner (private communication).

<sup>11</sup>D. H. Gloeckner and F. J. D. Serduke, Nucl. Phys. **A220**, 477 (1974).

<sup>12</sup>V. S. Shirley, in *Hyperfine Interactions in Excited Nuclei*, edited by G. Goldring and R. Kalish (Gordon and Breach, New York, 1971), Vol. 4, p. 1255.

<sup>13</sup>O. Häusser, I. S. Towner, T. Faestermann, H. R. Andrews, J. R. Beene, D. Horn, D. Ward, and C. Broude, contribution to The IV International Conference on Hyperfine Interactions, Madison, 1977 (unpublished).